SEGMENTATION OF THE ULTRASOUND IMAGES OF BREAST CANCER BY GENERALIZED GRADIENT VECTOR FLOW SNAKES

Stanislav S. Makhanov

School of Information and Computer Technology, Sirindhorn International Institute of Technology, Thammasat University, Thailand
e-mail: makhanov@siit.tu.ac.th

Abstract

The paper presents two new modifications of the Generalized Gradient Vector Flow Snakes based on the directional analysis of the corresponding vector field.

Keywords: medical image processing, segmentation, breast cancer, ultrasound

Introduction

Segmentation of ultrasound (US) images of breast cancer is one of the most challenging problems of the modern medical image processing. A number of popular codes for US segmentation are based on a generalized gradient vector flow (GGVF) method proposed by Prince and Xu [1]. A "raw" gradient vector field derived from the image edges is replaced by a field which minimizes a certain variational functional. The functional is designed to extend the large gradients far from the boundary, smooth the noise and speckles while keeping gradients attached to strong edges (see a fairly comprehensive review [2]).

The Euler system for the functional includes two elliptic equations which are interpreted as a steady state diffusion of the gradient vector flow. However, the GGVF does not take into account relative orientations of the vectors. Therefore, certain configurations, for instance, parallel vectors with large magnitude will not be smoothed although they do not form a boundary. Furthermore, a weak true boundary can generate a sequence of antiparallel vectors having small magnitudes. Such vectors may be destroyed by the diffusion. Consequently, the edge will be damaged and the snake will attach itself to a false boundary.

The Continuous Orientation Force Field Analysis(COFFA) [2] solves this problem by converting the vector field at every step of the iterative process back into the gray level and modifying the diffusion coefficients accordingly.

In this paper COFFA has been improved in such a way that it admits internal boundaries where the vector flow is temporarily or permanently fixed ("frozen boundaries"). The GGVF diffusion equation is then solved in the rectangular domain with the internal boundaries characterized by the Dirichlet boundary conditions(COFFA-GGVF-FB).

Furthermore, we propose to equip the GGVF equations with a diffusion coefficient which is polynomial function of the intensity of the edge map. The procedure generates clusters corresponding to the background, the shadows/noise and the boundary. The centers of the clusters are used to interpolate the diffusion to obtain it for an arbitrary gray level. At this step we apply a monotone polynomial interpolation which works better than the exponential diffusion used by the standard GGVF(COFFA-GGVF-FB-DYK).

Continuous Orientation Field Flow Analysis

The improved version of the GVF [1] is called the generalized gradient vector flow GGVF [5]. The weighting functions g and h depend on the gradient of the edge map so that in the proximity of large gradients g gets smaller whereas h becomes larger. The GGVF model is given by

$$\frac{\partial V}{\partial t} - g\left(|\nabla f|\right)\nabla^2 V - h\left(|\nabla f|\right)(\nabla f - V) = 0 .$$

where ∇f is the gradient field derived from the edge map of the image. For instance, $f = |\nabla I|$, where I is the gray level of the edge map. A variety of edge detectors such as the Canny or Sobel detectors can be applied to evaluate $|\nabla I|$ and

$$g\left(|\nabla f|\right) = e^{-\left(|\nabla f|/K\right)}, \quad h\left(|\nabla f|\right) = 1 - g\left(|\nabla f|\right),$$ where K is a calibration parameter.

In this paper we modify function g as follows

$$g\left(s_M, s_D\right) = e^{-F_M\left(s_M\right)F_D\left(s_D\right)},$$

where s_M, s_D is the magnitude and direction score of the vector field respectively and F_M, F_D are the corresponding score functions.

At the boundary of the object the vector field consists of antiparallel vectors. In this case the diffusion coefficient $g\left(s_D, s_M\right)$ must be small and "stopping coefficient" $h\left(s_D, s_M\right)$ must be large. As opposed to that, parallel vectors corresponding to the background should entail large diffusion, so that the small noise is smoothed and the large gradients along the boundary propagate through this area. In order to capture the direction along which the vectors are aligned the most, the algorithm introduces a rotating window. For each orientation of the window the vector field is first interpolated into the corners of the window

Next, $\varphi(\theta_1, \theta_2)$ measures the deviation of the vectors at the two opposing corners from the direction corresponding to the orientation of the window. The closer the two vectors are to the prescribed direction the greater is $\varphi(\theta_1, \theta_2)$.

The maximum response $\varphi(\theta_1, \theta_2)$ shows how close to the anti-parallel position the vector field is in the locality of the candidate boundary point. In order to construct the membership function $\varphi(\theta_1, \theta_2)$ we use two dimensional interpolation techniques with a few control points.

The measure $\varphi(\theta_1, \theta_2) : ([0, 2\pi] \times [0, 2\pi]) \to [0, 1]$ is constructed on a triangle $\left\{ \left(0, \dfrac{\pi}{2}\right), \left(\dfrac{\pi}{2}, \dfrac{\pi}{2}\right), \left(\dfrac{\pi}{2}, \pi\right) \right\}$ using interpolating points at the corners and in the middle of each side of the triangle. The following conditions at the interpolating points are used:

$$\varphi(0, \pi) = 1, \; \varphi\left(\dfrac{\pi}{2}, \pi\right) = 0, \; \varphi\left(\dfrac{\pi}{4}, \dfrac{3\pi}{4}\right) = \beta, \; \varphi\left(0, \dfrac{3\pi}{4}\right) = \alpha, \; \varphi\left(\dfrac{\pi}{2}, \dfrac{\pi}{2}\right) = 0, \; \varphi\left(\dfrac{\pi}{2}, \dfrac{3\pi}{4}\right) = 0,$$

where α and β are the design values (see Figure 1. (a) - (f) respectively).
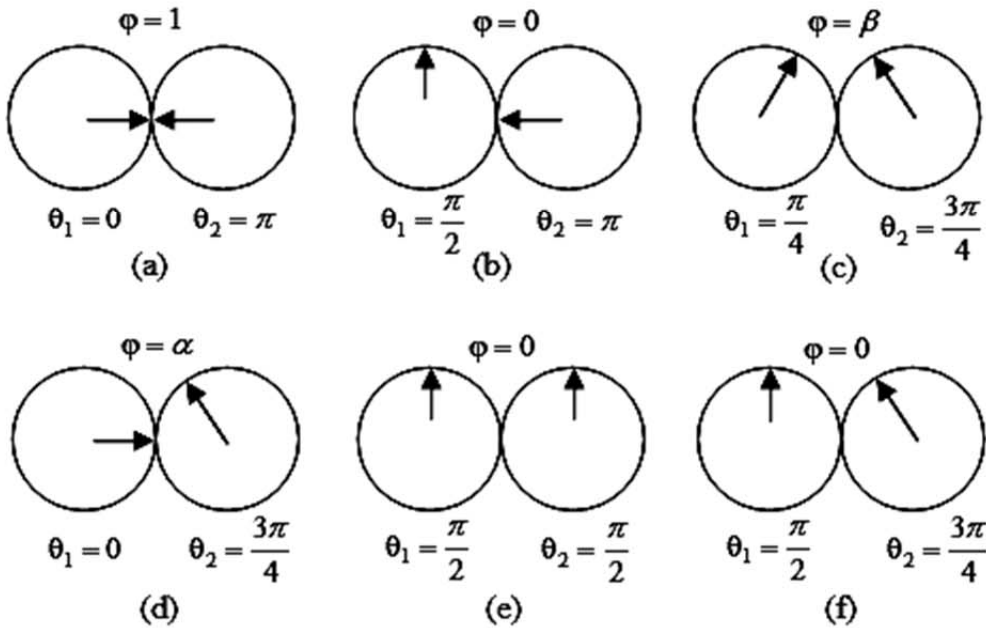

Figure 1 (a)-(f) The standard positions

Furthermore, the six positions define a quadratic polynomial given by

$$\varphi(\theta_1, \theta_2) = a_1 \theta_1^2 + a_2 \theta_1 \theta_2 + a_3 \theta_2^2 + a_4 \theta_1 + a_5 \theta_2 + a_6.$$

Once coefficients a_i are evaluated, $\varphi(\theta_1, \theta_2)$ is extended to $[0, 2\pi] \times [0, 2\pi]$ symmetrically, thus, becoming a piecewise quadratic function. Furthermore, $\varphi(\theta_1, \theta_2)$ applies to rotating window to produce a sequence of two dimensional score vectors $s_\gamma = (\varphi_1, \varphi_2)_\gamma$, where γ is the rotation angle.

The vectors are normalized as follows $s_{\gamma, new} = \dfrac{s_\gamma}{\max | s_\gamma |}$. Finally, the directional score $s_D = \min_\gamma | s_{\gamma, new} |$. We assume that the true contour points form large clusters characterized by $s_D > 1 - \delta$, where δ is an appropriate threshold. Besides the true boundary points must belong to relatively large continuous segments, whereas the false contour points belong to short segments. Consequently, appropriate edge detection methods can be applied.

Adaptive Diffusion Coefficients

Recall the diffusion coefficient given by $g(s_M, s_D) = e^{-F_M(s_M) F_D(s_D)}$.

As opposed to the classical GGVF where $g(s_M) = e^{-\frac{s_M}{K}}$, where K is a single tuning parameter, our model employs a rational function $F_M(s_M) = -\frac{s_M}{K(s_M)}$, where $K(s_M)$ is a monotone Hermite cubic spline such that $K(s_M) < 0, \forall s_M$. The polynomial is generated using significant clusters of the edge map. The clusters are generated by the standard fuzzy C-mean method.

Usually, our algorithm generates four clusters corresponding to background, noise, shadows and the boundary of the tumor. The centroid of each cluster is selected as the representative of the cluster and the corresponding Hermite polynomial is constructed so that $F_M(s_i) = \zeta_i$, where ζ_i are selected manually. However, if the cluster of shadows is not well defined, only three clusters are generated. Finally, $F_M(0) = 0$. Therefore, if gradient of the edge map is equal to zero, the diffusion reaches its maximum $g(s_M, 0) = 1$. The Hermite polynomial is the monotone piecewise cubic Fritsch-Carlson spline [4]. constructed using the slopes of the secant lines between the successive points and adjusting the slopes to ensure monotonicity.

Numerical Experiments

This section presents numerical experiments tested on a ground truth contours obtained from a series of breast tumor US images. The ground truth was hand-drawn by leading radiologists with Queen Sirikit Center for Breast Cancer of Bangkok.

This section compares the classic GGVF method with the method described above. Let us denote the proposed method by COFFA-GGVF-FB-DYK where FB stands for the frozen boundary and DYK for the dynamic choice of K combined with the Hermite interpolation [4]

In order to be fair to the conventional GGVF we run it on the same preprocessed images and find the best K by using a grid search. Finally, the preprocessing employs the same set of parameters defined by training, even though for some images it is possible to find a better combination of the parameters.

The accuracy is defined as a percentage of true positive points with the reference to the true boundary. A contour point is considered to be a true positive point if a point in the ground truth image belongs to the true contour.

The accuracy is also evaluated in terms of the generic Hausdorff distance (H_1) given by

$$\text{dist}_{H_1}(X,Y) = \max\{\max_{a \in X} \min_{b \in Y} \|a-b\|, \max_{b \in Y} \min_{a \in X} \|a-b\|),$$

where $\|\ \|$ denotes the Euclidian distance, X the ground truth contour and Y the resulting contour. The averaged Hausdorff distance (H_2) is obtained from (12) by replacing the

internal maximum by averaging. In order to obtain a dimensionless estimate (H_3) the Hausdorff distance is divided by the length of the true contour. In order to eliminate zeros after the decimal point in the forthcoming tables the normalizing coefficient for in H_3 is 1000.0 .

A combination of the true positives and the Hausdorff distance is a good measure of the segmentation quality. A larger degree of overlap of the boundaries (true positives) signifies a better segmentation. On the other hand, if the number of true positives is equal to zero, the boundaries could still be close, say at the distance of one pixel. In that case the Hausdorff distance shows that the quality of segmentation is still relatively good. In turn, a set of boundaries dissimilar only over small portions may have the same Hausdorff distance as that of the globally dissimilar set of boundaries. However, if the boundaries are globally dissimilar we may expect a very low number of true positives. Finally, if the number of true positives is high and the Hausdorff distance is low, the quality of segmentation is very likely to be good. We also evaluate the robustness of the method by its numerical convergence.

Example 1 Low Contrast Malignant Tumor

Figure 2(a) displays the original US image. Figure 2(b) shows the segmentation by conventional GGVF. The ground truth images such as in Figure 2(b) were outlined by Dr. Mavin Wongsaisuvan, who is currently a leading radiologist with the Queen Sirikit Center for Breast Cancer of King Chulalongkorn Memorial Hospital, Bangkok Thailand. The results obtained with two versions of the proposed COFFA-GGVF are shown in Figures 2 (c) and (d). The numerical evaluation of the accuracy of the extractions is given in Table 2. The accuracy is estimated in terms of true positives(TP) and the Hausdorff distance .
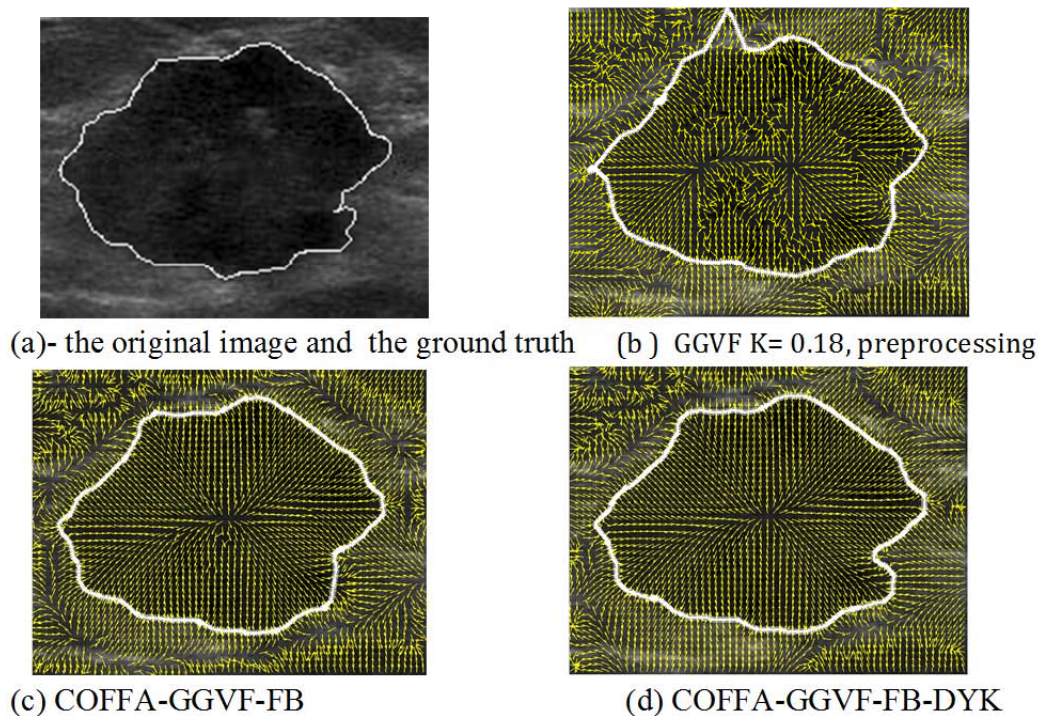

(a)- the original image and the ground truth   (b) GGVF K= 0.18, preprocessing

(c) COFFA-GGVF-FB   (d) COFFA-GGVF-FB-DYK

Figure 2 Extraction results using the proposed method with the reference to the standard GGVF.

Table 1 indicates convergence of the methods and the best accuracy throughout 5,000 iterations. Since the conventional GGVF often does not converge, the best accuracy was recorded at some transitional iteration step. However, a criterion to terminate the GGVF iterations if they do not converge in the classical sense is an open problem. Therefore, the GGVF accuracy is actually overestimated. Still our proposed method outperforms GGVF. First of all, it always converges. Second, COFFA-GGVF-FB-DYK with the adaptive K outperforms GGVF endowed with the best K found by the trial end error method, where $g = e^{-\frac{|\nabla f|}{K}}$ and g is the diffusion. As opposed to that the adaptive method does not require any training and will adapt K automatically. Note that K employs a monotone Hermite spline interpolation [4]

For GGVF and the proposed method the classical explicit numerical scheme was employed which converges if $4g_{max} < 1$ [1] . This condition was satisfied for every experiment. However, GGVF iterations may also diverge when $g(|\nabla f|)$ is too small, that is, the parabolic equation degenerates. This case requires special numerical procedures for parabolic equations with singularities. For instance, if $g(|\nabla f|) \equiv 0$, the system is no longer parabolic. Therefore, boundary conditions (required for uniqueness of the solution of the parabolic equation) can not be satisfied.

However, the proposed polynomial interpolation does not change as fast as the exponential diffusion. Besides we freeze the numerical solution when $g(|\nabla f|)$ is close to zero. These procedures help to maintain the numerical stability and provide the convergence even when the simple explicit scheme is employed

Finally, in many cases the accuracy of GGVF is very sensitive to variations of K. Consider a graph of TP vs. K in Figure 3. The maximum accuracy $TP_{max} = 89\%$ is achieved at $K=0.185$. Let us define an acceptable range as $\{K : TP \leq 0.99 TP_{max}\}$. Then $K \in [0.17, 0.225]$ with the average accuracy 88% within this interval. It is a relatively large interval, however, the accuracy drops abruptly when $K < 0.17$. For instance, for $K=0.16$ the accuracy is only 62%.

The adaptive procedure endowed by COFFA and FB increases the variability of the permissible diffusion $g(s)$, thus, resulting in the same or even better segmentations with the reference to the best GGVF performance.

Note that the best maximum Hausdorff error $H_1 = 5.0$ pixels which seems large. However, the best average Hausdorff error $H_2 = 1$. It means that on average, the actual contour deviates from the true contour by only 1 pixel.

Table 1 Accuracy and convergence of GGVF and COFFA-GGVF-DYK-FB

| Method / Criterion	No-preprocessing GGVF, best K=0.13	Preprocessing GGVF, K varied 0.18 max accuracy	Acceptable range: 0.17-0.22	GGVF-DYK	COFFA-GGVF-FB-DYK
TP	39.1975	89.1901	88.0814	91.3580	93.0329
Hausdorff max, H_1	23.2402	8.1519	8.9413	6.1855	5.1173
Hausdorff average, H_2	9.1462	1.0329	1.0724	0.9059	0.7638
Snake convergence	Yes	yes	Yes	yes	yes
GGVF convergence explicit scheme	No	no	No	yes	yes
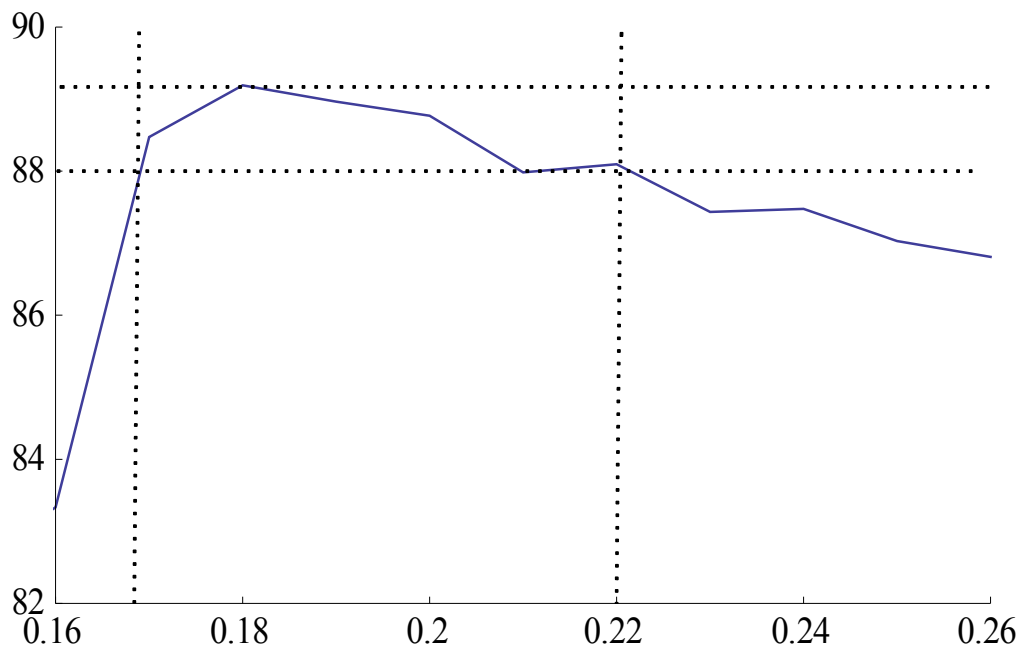
Figure 3 Accuracy of GGVF vs. the diffusion coefficient *K*.

Consider segmentation results presented in Figure 2. Clearly, GGVF—DYK and COFFA-GGVF-FB-DYK generate star-like patterns ideal for using the expanding snakes whereas GGVF with the best *K*=0.185 generates multiple stars (unwanted internal boundaries). Finally, only COFFA-GGVF-FB-DYK is able to resolve the corner on the right side of the image.

Finally, let us analyze the accuracy vs. the iteration number in Figure 4. The standard GGVF does not converge whereas the proposed method does.
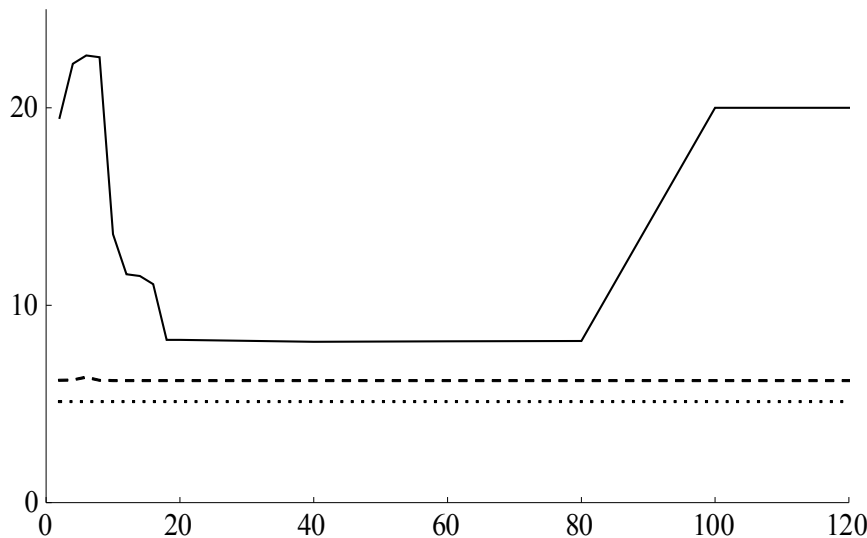
Figure 4 Convergence: H_1, solid line – GGVF, dashed line COFFA-GGVF-DYK, dotted line COFFA-GGVF-DYK-FB

The accuracy of GGVF in terms of TP reaches its peak at 6th -9th iteration. However, the diffusion destroys the boundary decreasing the number of true positives. The maximum Hausdorff distance stays stable for some number of iterations. However, once the location of the maximum error changes, the accuracy in terms of H_1 abruptly drops (Figure 4). As opposed to that H_2 based on the averaging the distances, changes smoothly. However, it increases starting with 16th -18th iteration. In any case, neither TP nor H_1, H_2 converge. As opposed to that, both versions of the proposed method converge, that is, after a few iterations the vector field remains the same indefinitely.

Example 2 A medium contrast malignant tumor. Complicated Shape. High Noise.

Results similar Example 1 are obtained for a malignant tumor in Figure 5 (a). Table 2 shows that COFFA-GGVF-FB-DYK outperforms the standard GGVF even for the best K selected manually.

Note that optimal K for GGVF for Example 2 is very different from K obtained in Example 1. The optimal $K=0.18$ for the tumor from Example 1, however the best $K=0.13$ for Example 2. Moreover, the acceptable range in Example 1 and 2 is [0.17-0.22] and [0.12-0.13] respectively. The high variability of optimal K in (compare Figure 3 and Figure 6) means that it might not be possible to always establish a single K for GGVF model even by training the model on a series of images. Nevertheless, the proposed model is parameter free. The dynamic K is established automatically and varies from region to region.
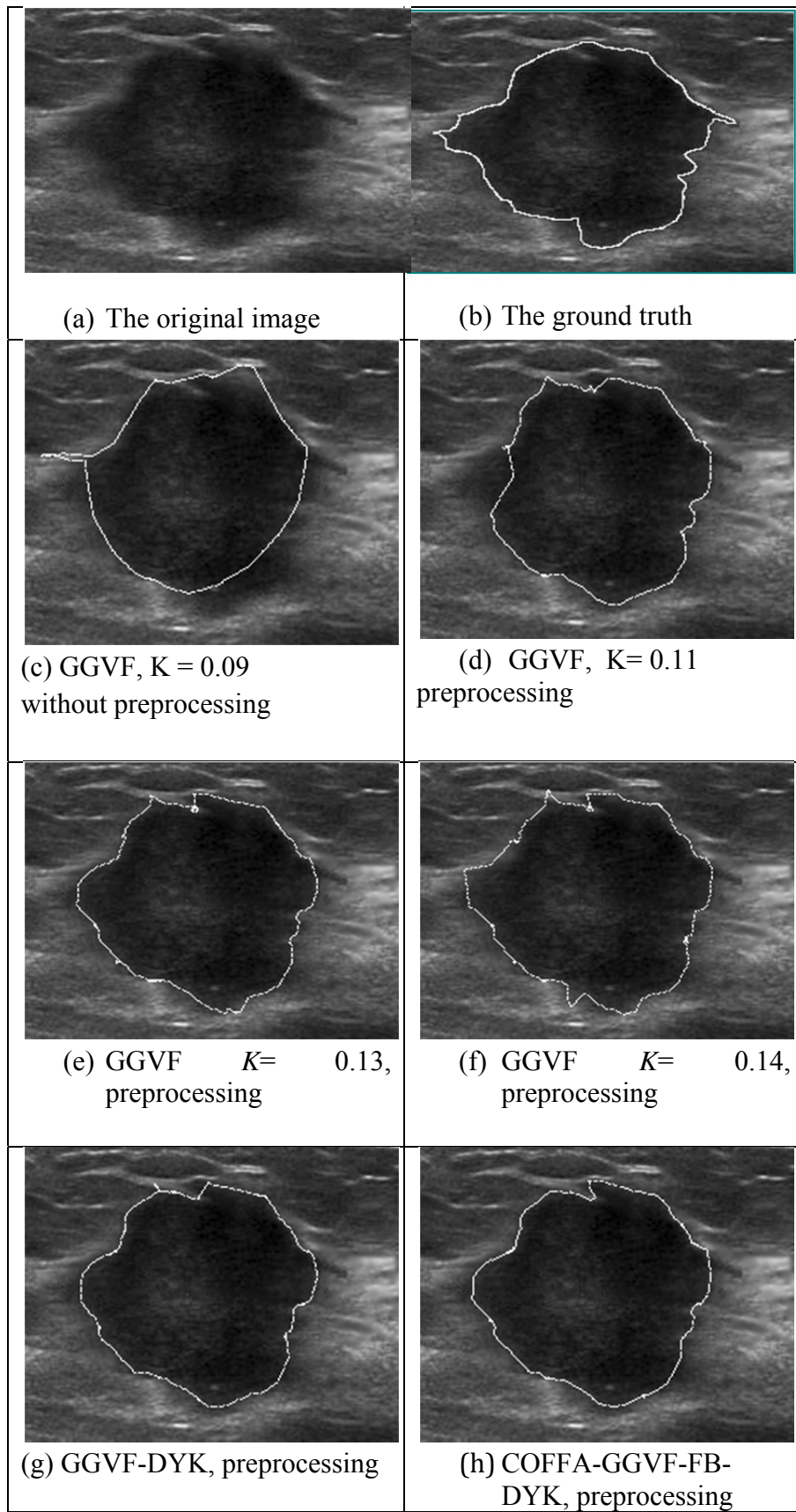
(a) The original image

(b) The ground truth

(c) GGVF, K = 0.09 without preprocessing

(d) GGVF, K= 0.11 preprocessing

(e) GGVF $K=$ 0.13, preprocessing

(f) GGVF $K=$ 0.14, preprocessing

(g) GGVF-DYK, preprocessing

(h) COFFA-GGVF-FB-DYK, preprocessing

Figure 5 Extraction results using the proposed method with the reference to the standard GGVF.

Table 2 Accuracy and convergence of GGVF and COFFA-GGVF-DYK-FB

Method / Criterion	No preprocessing GGVF + best K 0.09	Preprocessing GGVF _K_ varies Best K=0.13	Acceptable range: K=0.12-0.134	GGVF-DYK	COFFA-GGVF-FB-DYK
TP HD1 HD2 HD3	24.9165 32.0278 23.9605 13.4837	88.0059 7.0881 1.3935 0.7841	88.0050 7.3531 1.3939 0.7843	88.2698 6.6123 1.3660 0.7687	91.0236 5.6857 0.6766 0.3808
Snake convergence	yes	yes	yes	yes	yes
GGVF convergence	no	no	no	yes	yes

Again the proposed approach over performs the conventional GGVF and converges to a meaningful solution.
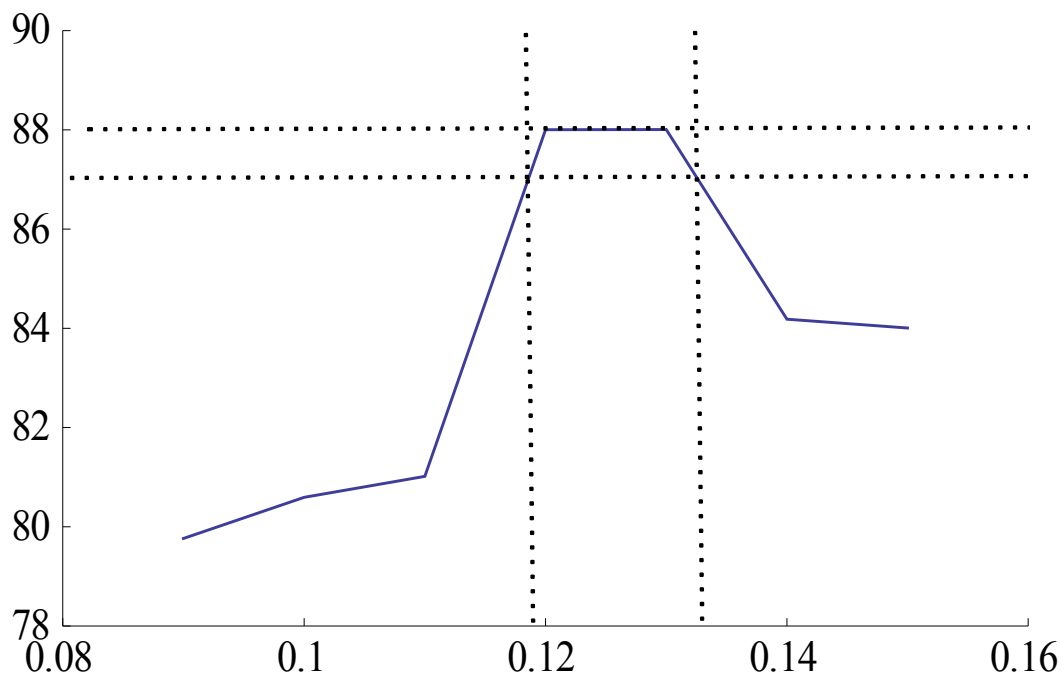

Figure 6 Accuracy of GGVF vs. the diffusion coefficient _K_.

Conclusions

The proposed adaptive GGVF-COFFA-FB-DYK snake shows much promise as applied to detection breast tumors in ultrasound images. The method provides the same or better accuracy with the reference to the conventional GGVF equipped with the best parameters. The model is less sensitive with regard to the distance between the initial contour and the object boundary. The method can be applied with a variety of edge detection methods and in many cases the required thresholds can be selected automatically.

Acknowledgement

References

1. C. Xu and J.L. Prince, Snakes, shapes, and gradient vector flow, IEEE Transaction on Image Processing. Vol. 7 (3), 1998, pp. 359–369
2. A. Rodtook and S. S. Makhanov, Continuous force field analysis for generalized gradient vector flow field, Pattern Recognition, vol. 43(10), 2010, pp. 3522 – 3538
3. J. S. Lee, Digital image enhancement and noise filtering by using local statistics, IEEE Transactions in Pattern Analysis and Machine Intelligence, PAM1-2, 1980, pp.165-168
4. F.N Fritsch and R.E. Carlson, Monotone Piecewise Cubic Interpolation, SIAM J. of Numerical Analysis, 17, 1980, pp. 238-246
5. C. X and J.L. Prince, Generalized gradient vector flow external forces for active contours, Signal Processing, 71 (2), 1998, pp. 131-139